Determination of in vivo oxygen uptake and carbon dioxide evolution rates from off-gas measurements under highly dynamic conditions

Wu, L.; Lange, H. C.; Van Gulik, W. M.; Heijnen, J. J.

DOI
10.1002/bit.10480

Publication date
2003

Document Version
Final published version

Published in
Biotechnology and Bioengineering

Citation (APA)
Wu, L., Lange, H. C., Van Gulik, W. M., & Heijnen, J. J. (2003). Determination of in vivo oxygen uptake and carbon dioxide evolution rates from off-gas measurements under highly dynamic conditions. *Biotechnology and Bioengineering*, *81*(4), 448-458. https://doi.org/10.1002/bit.10480

Determination of in Vivo Oxygen Uptake and Carbon Dioxide Evolution Rates from Off-gas Measurements Under Highly Dynamic Conditions

L. Wu, H. C. Lange, W. M. van Gulik, J. J. Heijnen

Kluyver Laboratory for Biotechnology, Delft University of Technology, The Netherlands

Received 26 July 2001; accepted 2 July 2002

DOI: 10.1002/bit.10480

Abstract: In vivo kinetics of *Saccharomyces cerevisiae* are studied, in a time window of 150 s, by analyzing the response of O_2 and CO_2 in the fermentor off-gas after perturbation of chemostat cultures by metabolite pulses. Here, a new mathematical method is presented for the estimation of the in vivo oxygen uptake rate (OUR) and carbon dioxide evolution rate (CER) directly from the off-gas data in such perturbation experiments. The mathematical construction allows effective elimination of delay and distortion in the off-gas measurement signal under highly dynamic conditions. A black box model for the fermentor off-gas system is first obtained by system identification, followed by the construction of an optimal linear filter, based on the identified off-gas model. The method is applied to glucose and ethanol pulses performed on chemostat cultures of *S. cerevisiae*. The estimated OUR is shown to be consistent with the independent dissolved oxygen measurement. The estimated in vivo OUR and CER provide valuable insights into the complex dynamic behavior of yeast and are essential for the establishment and validation of in vivo kinetic models of primary metabolism. © 2003 Wiley Periodicals, Inc. *Biotechnol Bioeng* **81**: 448–458, 2003.

Keywords: oxygen uptake rate; carbon dioxide evolution rate; pulse experiment; *Saccharomyces cerevisiae;* in vivo kinetics; system identification

INTRODUCTION

Targeted alteration of metabolic pathways by recombinant DNA techniques allows the redirection of metabolic fluxes towards desired final products (Lessard, 1996). Prediction of the targets and the outcomes of these alterations is impeded, however, by intrinsic nonlinearity of biological systems, which calls for the application of mathematical models to cellular metabolism (Bailey, 1998). Kinetic models, which combine enzyme kinetics with known stoichiometry of metabolic pathways, have proven useful in describing and understanding the global dynamic behavior of microbes (Gombert and Nielsen, 2000). The importance of using in vivo enzyme kinetics in this kind of models, instead of in vitro kinetics, has been illustrated by Wright et al. (1992) and Teusink et al. (2000).

In vivo enzyme kinetics can be evaluated by pulse experiments, during which a substrate pulse is administered to a steady-state chemostat culture (Theobald et al., 1997). The responses of the culture are observed in a short time window, e.g., 100–200 s after the pulse, to ensure approximately constant enzyme levels. Analysis of intra- and extracellular metabolite concentrations within this time frame allows the estimation of in vivo kinetic parameters (Rizzi et al., 1997; Vaseghi et al., 1999) or the validation and diagnosis of the entire kinetic model (Visser et al., 2000).

In addition to metabolite concentrations, continuous measurements of oxygen and carbon dioxide content in the fermentor off-gas or the fermentation broth can be obtained from online sensors, which facilitate in principle the estimation of the in vivo oxygen uptake rate (OUR) and carbon dioxide evolution rate (CER). Both are closely related to the primary metabolism, either through the respiratory chain or reactions in the pyruvate branch point, the TCA cycle, and the PP pathway. Despite their relevance to kinetic modeling, estimation of the OUR and CER during transient, in the time scale of 100–200 s, has not been reported previously in the field of metabolic engineering.

Instead, nonstationary OUR estimation has been addressed in wastewater treatment processes, utilizing dissolved oxygen (DO) measurement. Both instrumental (e.g., respirometry) and software sensors have been applied. A continuous respiratory meter suffers from large calculation intervals (typically 60 s) (Spanjers et al., 1994). With software sensors, a constant (oxygen) partial pressure in the gas phase is assumed (Holmberg and Olsson, 1989; Carlsson et al., 1994). Recursive least square techniques or Kalman filtering have been applied to estimate the OUR and the oxygen mass transfer coefficient (k_La) simultaneously, the latter being modeled as a function of the gas flow rate. Lindberg and Carlson (1996) used a polynomial filtering method to reduce the influence of DO sensor dynamics.

In the case of pulse experiments, the assumption of a constant gas phase O_2 and CO_2 partial pressure no longer holds. Sudden changes in the OUR and CER lead to dy-

namics in the mass transfer between the liquid and gas phase in the fermentor and consequently to rapid changes in the gas partial pressure. Coupled mass balances for O_2 and CO_2 in the liquid and gas phase are therefore required for the reconstruction of OUR and CER during pulse experiments.

The gas-phase O_2 and CO_2 partial pressure is monitored as the volume fractions in the fermentor off-gas, while the dissolved oxygen and carbon dioxide (DO and DCO_2) can be measured closer to the source. The DO and DCO_2 measurements have several drawbacks, however:

- DO or DCO_2 sensors are prone to drift and fouling, which cannot be easily corrected by repeated calibration during fermentations.
- The DCO_2 sensors based on a pH difference measurement are impractical for use in continuous cell cultivation (Pattison et al., 2000), while commercial fiber optic DCO_2 probes do not provide sufficient sensitivity in the concentration range of interest (typically under 5% partial pressure of CO_2). The CER estimation therefore solely depends on off-gas CO_2 measurement.

Moreover, off-gas measurements can be easily extended to volatile metabolites by other detection methods, such as mass spectrometry.

During transient, the off-gas measurement does not reflect the actual gas partial pressures in the fermentor gas phase. The off-gas system in a conventional fermentation setup (see Fig. 1) contains large dead volumes, such as headspace and tubing, which cause mixing effects and a time delay. The measured signal is further influenced by sensor dynamics and process and measurement noises.

Taking account of these effects, a new approach is presented in this paper to estimate the OUR and CER during pulse experiments in a time window of 150 s, using off-gas measurements. The method is based on the identification of an input–output transfer function model for the off-gas system, followed by the construction of a linear polynomial filter as described by Lindberg and Carlsson (1996). The practical application of this new approach is demonstrated with glucose and ethanol pulse experiments on chemostat cultures of *Saccharomyces cerevisiae*.

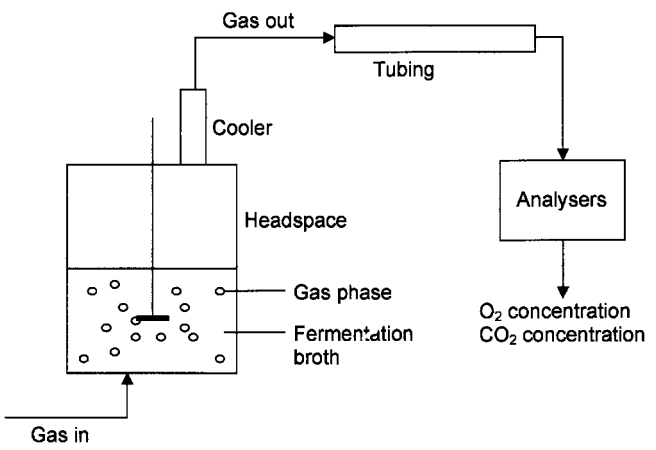

Figure 1. Schematic depiction of the off-gas system.

THEORETICAL ASPECTS

Model Development

Both the liquid and gas phase (that is, the gas present as gas bubbles in the fermentation broth) in the fermentor are described as ideally mixed CSTRs with the following set of differential equations.

Gas phase:

$$V_G \frac{dc_G}{dt} = \Phi_G(c_{G,in} - c_G) - k_L a \cdot V_L \left(\frac{c_G}{m} \frac{P}{P_0} - c_L \right) \quad (1)$$

Liquid phase:

$$\frac{dc_L}{dt} = \frac{\Phi_L}{V_L}(c_{L,in} - c_L) + k_L a \left(\frac{c_G}{m} \frac{P}{P_0} - c_L \right) + r \quad (2)$$

In Eq. (1) the gas flow rates in and out of the fermentor are assumed to be constant. At an operating pH of 5, the concentration of carbonate ion is negligible and only dissolved carbon dioxide will contribute to the mass transfer (Royce and Thornhill, 1991). Furthermore, the term

$$\frac{\Phi_L}{V_L}(c_{L,in} - c_L)$$

can be neglected in further analysis, since the liquid flow rate is very small.

Further, it is assumed that the complex mixing effects of the off-gas in different compartments (e.g., the headspace, the cooler, the tubing system, etc.) can be approximated by a *finite* number of CSTRs in a series, all with appropriate dimensions. The model equation for the i^{th} CSTR in the series of CSTRs is given by

$$\frac{dc_i}{dt} = \frac{1}{\tau_i}(c_{i-1} - c_i), \quad i = 1, 2, \ldots, N \quad (3)$$

where c_i and τ_i are the gas concentration and the residence time of the i^{th} CSTR, respectively. c_0 corresponds to the O_2 or CO_2 concentration in the gas bubbles, which enter the headspace.

The dynamics of the off-gas analyzer is assumed to be first order and given by

$$\frac{dx}{dt} = \frac{1}{\tau_a}(c_N - x) \quad (4)$$

where τ_a is the first-order analyzer constant and x the measured gas concentration. The final measurement y is given by

$$y(t) = x(t - k) \quad (5)$$

where k is the combined net time delay produced by the dead volumes in the off-gas system. The modeling steps above are shown schematically in Figure 2.

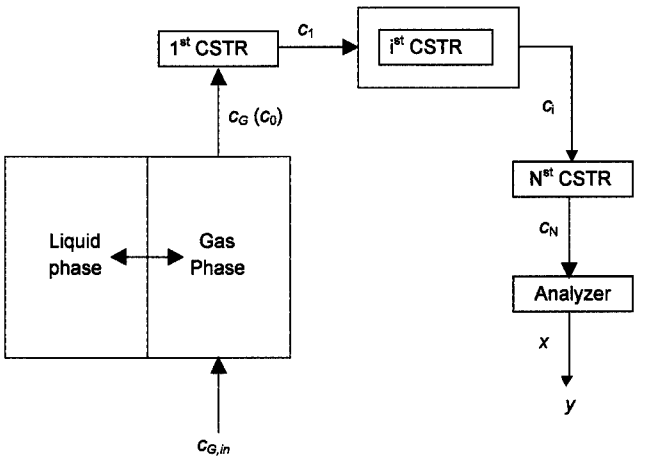

Figure 2. Modeling of the off-gas system.

Laplace transformation of Eqs. (1)–(5), assuming steady-state initial conditions [i.e., all derivatives are zeros in Eqs. (1)–(5)] yields:

$$c'_{\mathrm{G}}(s) = \frac{B_1(s)}{F(s)}\, c'_{\mathrm{G,in}} + \frac{B_2}{F(s)}\, r'(s) \tag{6a}$$

$$y'(s) = e^{-\mathrm{sk}}\, \frac{G_{\mathrm{n}}}{G_d(s)}\, c'_{\mathrm{G}}(s) \tag{6b}$$

Here, the prime denotes a deviation from the steady state (e.g., $y' = y - y^0$). The definitions of all transfer functions are given in Appendix 1.

Combining 6a and b by eliminating $c'_{\mathrm{G}}(s)$ yields

$$\begin{aligned} y'(s) &= e^{-\mathrm{sk}}\, \frac{G_n}{G_d(s)}\, \frac{B_1(s)}{F(s)}\, c'_{\mathrm{G,in}}(s) + e^{-\mathrm{sk}}\, \frac{G_n}{G_d(s)}\, \frac{B_2}{F(s)}\, r'(s) \\ &= e^{-\mathrm{sk}}\, \frac{B_c(s)}{A(s)}\, c'_{\mathrm{G,in}}(s) + e^{-\mathrm{sk}}\, \frac{B_r}{A(s)}\, r'(s) \\ &= G_c(s) c'_{\mathrm{G,in}}(s) + G_r(s) r'(s), \end{aligned} \tag{7}$$

where

$$B_c(s) = G_n \cdot B_1(s), \quad B_r = G_n \cdot B_2, \quad A(s) = G_d(s) \cdot F(s),$$

$$G_c(s) = e^{-\mathrm{sk}}\, \frac{B_c(s)}{A(s)}, \quad G_r(s) = e^{-\mathrm{sk}}\, \frac{B_r}{A(s)}. \tag{8}$$

Since off-gas measurements are registered by a digital computer at discrete time intervals, it is convenient to rewrite Eq. (7) in a discrete fashion. With the introduction of the forward shift operator q defined by

$$qf(nT) = f(nT + T) \tag{9a}$$

and the backward shift operator q^{-1} defined by

$$q^{-1} f(nT) = f(nT - T) \tag{9b}$$

the discrete time transfer functions can be obtained by approximation of s in the continuous time transfer functions with Euler's method, when the sampling interval T is short:

$$s \approx \frac{q-1}{T} \tag{10}$$

Assuming that corruption of the measurement can be described by white noise $e(t)$, a combination of Eqs. (7), (9a,b), and (10) gives the final discrete-time input–output transfer function model of the off-gas system:

$$y'(t) = G_c(q) c'_{\mathrm{G,in}}(t) + G_r(q) r'(t) + H(q) e(t), \tag{11}$$

where

$$G_c(q) = q^{-\mathrm{k}}\, \frac{B_c(q)}{A(q)}, \quad G_r(q) = q^{-\mathrm{k}}\, \frac{B_r}{A(q)}, \quad H(q) = \frac{C(q)}{D(q)},$$

and A, B, C, and D are polynomials in q^{-1}:

$$A(q) = 1 + a_1 q^{-1} + \cdots + a_{\mathrm{n_a}} q^{-\mathrm{n_a}}$$

$$B(q) = b_1 q^{-1} + \cdots + b_{\mathrm{n_b}} q^{-\mathrm{n_b}}$$

$$C(q) = 1 + c_1 q^{-1} + \cdots + c_{\mathrm{n_c}} q^{-\mathrm{n_c}}$$

$$D(q) = 1 + d_1 q^{-1} + \cdots + d_{\mathrm{n_d}} q^{-\mathrm{n_d}}$$

System Identification

The transfer functions in Eq. (11) contain a large number of unknown parameters, e.g., the number of CSTR's in series, their residence time τ_i, etc., (see also Appendix 1), the estimation of which will be extremely laborious, if not impossible. We therefore chose to treat the transfer functions as polynomials in q^{-1} with unknown polynomial coefficients, which no longer possess physical relevance. This "black box" approach allows the estimation of all coefficients with standard system identification techniques (Ljung, 1987). During system identification experiments the off-gas system is excited with known inputs while its response (output) is recorded. A linear quadratic estimate of the polynomial coefficients and time delay can be obtained with the input–output data.

According to Eq. (11), the off-gas system has two inputs, namely, the gas feed concentration $c_{\mathrm{G,in}}$ and the reaction rate r. The choice of the input used for system identification is however limited to $c_{\mathrm{G,in}}$, since the reaction rate r cannot be directly and precisely manipulated. Keeping r at a constant level during identification while varying $c_{\mathrm{G,in}}$ results in

$$y'(t) = G_c(q) c'_{\mathrm{G,in}}(t) + H(q) e(t) \tag{12}$$

which allows the identification of $G_c(q)$ and $H(q)$. $G_r(q)$ can be obtained from the identified $G_c(q)$ as follows.

Since the two transfer functions share the same denominator $A(q)$ and time delay k, the problem can be reduced to the determination of the scalar B_r, the nominator of $G_r(q)$. The gain $\mathcal{G}$ of the continuous or discrete transfer functions can be determined by taking $s = 0$ or $p = 1$. We thus have

$$\mathcal{G}_c = 1, \quad \mathcal{G}_r = \tau \tag{13}$$

Hence, using Eqs. (8) and (13) we obtain:

$$B_r = \tau \cdot A(s)|_{s=0} \quad \text{or} \quad B_r = \tau \cdot A(q)|_{q=1} \tag{14}$$

The gain relationship allows thus the identification of B_r.

For the actual "shape" of the input, the generalized binary sequence has been chosen (GBN, illustrated in Fig. 3). It is a stochastic signal, which randomly switches between two fixed levels at discrete points in time, with the nonswitching probability p defined as:

$$P(S_t = S_{t-1}) = p, \quad P(S_t \neq S_{t-1}) = 1 - p \tag{15}$$

The expectation of the switching interval T_{sw} is given by

$$E[T_{sw}] = \frac{T_b}{1-p} \tag{16}$$

where T_b is the length of a fixed basic switching interval.

The GBN can be easily implemented and is at the same time optimal for the statistical information content (Ljung, 1987). Our choice of p was guided by the global guideline outlined by Tulleken (1990), which leads to (sub)optimal GBN design in relation to *global* dynamic properties of the system to be identified. For a second-order overdamped system, the (sub)optimal nonswitching probability p satisfies

$$\frac{E[T_{sw}]}{\tau_s} = 1 \tag{17}$$

where τ_s is the 99% settling time. From the step response of the off-gas system it can be verified that the system is at least second order. Applying Eq. (17) yields (sub)optimal nonswitching probabilities, stated in Table I.

During identification, the GBN is realized by switching the concentration of O_2 or CO_2 in the gas feed between two constant values. The difference between these two levels has been chosen to cover as much as possible the concentration changes of O_2 or CO_2 in pulse experiments.

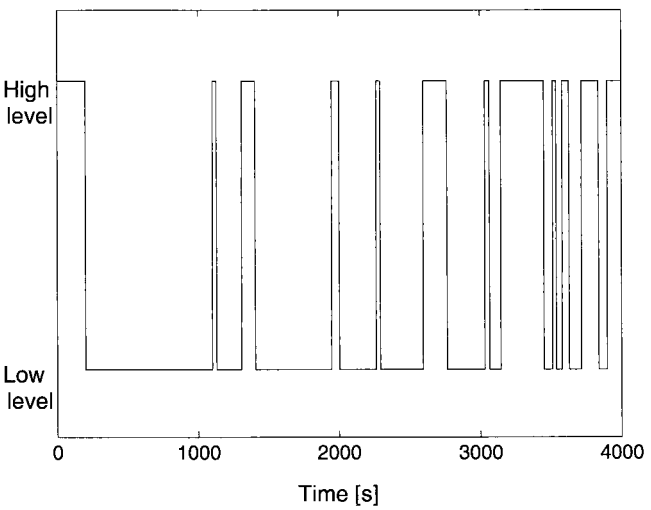

Figure 3. Random binary sequence with a fixed low input level and a fixed high input level.

Table I. Nonswitching probabilities used in system identification.

$C_{G,in}$	T_b (second)	p
O_2	3	0.98
CO_2	5	0.98

The off-gas system during identification should resemble as close as possible the off-gas system during perturbation experiments. This is partially satisfied due to the time-invariant physical properties of the components of the off-gas system, e.g., the headspace, cooler, tubing system, and analyzer. However, care has to be taken that the operational parameters, such as the stirring speed, pH, temperature, pressure, gas flow rate, liquid volume, and gas hold-up, are the same during the identification as during the pulse experiments. Additionally, the physical properties (such as density, viscosity, gas hold-up, and k_La, etc.) of the fermentor liquid phase used for identification should ideally be the same as those of a chemostat broth, which infers the use of a steady-state chemostat broth for identification experiments. A serious drawback is that the steady-state OUR and CER might be affected by step changes of the input gas concentrations. This is circumvented by using a resting cell culture as an alternative, which possesses approximately the same physical properties as the chemostat broth. The resting cell culture is obtained after switching off the medium feed to the chemostat for several hours, while the other cultivation conditions are kept unchanged.

Optimal Linear Filtering

Based on the identified transfer function $G_r(q)$, a linear filter can be constructed to estimate the actual reaction rates in a least-squares sense.

In the filtering problem the following linear system is defined:

$$y(t) = G(q)u(t) + H(q)e(t) \tag{18}$$

where

$$G(q) = q^{-k}\frac{B(q)}{A(q)}, \quad H(q) = \frac{C(q)}{D(q)},$$

$$u(t) = \frac{M(q)}{N(q)}v(t),$$

$$Ee(t)^2 = \lambda_e, \quad Ev(t)^2 = \lambda_v, \quad \text{and} \quad \rho = \lambda_e/\lambda_v$$

Here $e(t)$ and $v(t)$ are two independent stationary white and zero-mean noise processes; the noise to signal ratio ρ is defined as the quotient of their variances λ_e and λ_v. q^{-k} corresponds to a pure time delay in the transfer function $G(q)$ so that $B(q)$ does not contain any time delays. With the input model $M(q)/N(q)$, $u(t)$ is modeled as an auto-regressive moving average (ARMA) process.

A polynomial-based linear filtering method is used to estimate the input $u(t)$ by minimizing the mean square estimation error (Ahlén and Sternad, 1989):

$$E[\varepsilon(t)^2] = E[u(t) - \hat{u}(t|t-m)]^2 \tag{19}$$

For the estimation of reaction rates, m is negative and the filter corresponds to a fixed lag smoother. The optimal filter can be represented as

$$\hat{u}(t|t-m) = \frac{Q(q)}{R(q)}\, y(t-m) \tag{20}$$

The polynomials $Q(q)$ and $R(q)$ that attain the minimum value of Eq. (19) are given as

$$\frac{Q}{R} = \frac{Q_1 DA}{\beta} \tag{21}$$

where the backward shift operator q^{-1} is substituted by the complex argument z^{-1}, which is omitted for convenience.

With the definition of the polynomial P and its conjugate P_* as

$$P = P(z^{-1}) = 1 + p_1 z^{-1} + \cdots + p_{\mathrm{np}} z^{-\mathrm{np}}$$

$$P_* = P(z) = 1 + p_1 z + \cdots + p_{\mathrm{np}} z^{\mathrm{np}}$$

the polynomial factors Q_1 and β are obtained by solving first a spectral factorization:

$$R\beta\beta_* = MBDM_*B_*D_* + \rho CANC_*A_*N_* \tag{22a}$$

followed by a Diophantine equation (Ahlén and Sternad, 1989):

$$z^{m+k} M_* B_* D_* MC = R\beta Q_1 + zNL_* \tag{22b}$$

The choice of noise to signal ratio ρ in Eq. (22a) is a tradeoff between better tracking of changes in $u(t)$ (when ρ is small) and low variance in estimated $u(t)$ (when ρ is large). The optimal ρ is determined by tuning (Lindberg and Carlsson, 1996). This filtering method is equivalent to stationary Kalman filtering. But compared to the state space formulation of Kalman filtering, the design calculations are simpler, especially for systems with significant time delays and for smoothing problems.

For the off-gas system during perturbation, the reaction rates r are varying while the input gas concentration remains constant. We have, according to Eq. (11),

$$y'(t) = G_r(q) r'(t) + H(q) e(t) \tag{23}$$

Substitution of $y(t|t-m)$ with $y'(t|t-m)$ in Eq. (20) delivers the desired estimate of $r(t)$. To account for the varying nature of $r(t)$, the input model $M(q)/N(q)$ is parameterized as a random walk, which is widely used to model nonstationary time series (Grewal and Andrews, 1993):

$$\frac{M(q)}{N(q)} = \frac{1}{1 - q^{-1}} \tag{24}$$

MATERIALS AND METHODS

Organism and Chemostat Cultivation

S. cerevisiae CEN.PK 113-7D was cultivated in carbon-limited continuous cultures with a working volume of 4 L in a 7-L fermentor (Applikon, The Netherlands) at a dilution rate of about 0.05 h^{-1}. Conditions applied were a temperature of 30°C, a pH controlled at 5.0, a stirrer speed of 600 rpm, a gas feed (air) flow rate of approximately ¾ vvm, and an over-pressure of 0.3 bar. A doubled mineral medium (Verduyn et al., 1992) with 27.1 g/L glucose and 1.42 g/L ethanol was used to obtain approximately 15 g biomass (dry weight) per liter in steady state.

Model Identification Experiments

Identification experiments were performed in a resting cell culture. The GBN was realized by switching between two different levels of oxygen and carbon dioxide in the gas inlet (Table II). The oxygen and carbon dioxide contents in the off-gas were measured by a NGA200 gas analyzer (Rosemount Analytics, USA). The dissolved oxygen tension (DOT) was measured by a Mettler Toledo DOT sensor (Mettler-Toledo GmbH, Switzerland). The sampling rate of all measurements was 1 s^{-1}. Estimation of the polynomial coefficients was carried out with the Matlab 5.3 system identification toolbox.

Pulse Experiments

Under steady-state conditions, a pulse of glucose or ethanol was injected into the chemostat with a syringe to give an initial liquid-phase concentration of 1 g/L glucose or 0.5 g/L ethanol. The injected volume is negligible compared to the broth volume. Two glucose pulses were conducted on duplicate chemostat cultures G1 and G2. Two ethanol pulses were conducted on duplicate chemostat cultures E1 and E2.

RESULTS AND DISCUSSION

Chemostat Cultivation

Pulse experiments were performed on four separate chemostat cultures. Steady-state conditions were checked routinely via biomass concentration and off-gas analysis (Table III). All carbon and redox balances closed within ±3%.

Table II. Concentration in the gas feed used during identification.

	$\%O_2$		$\%CO_2$	
	High level	Low level	High level	Low level
Gas/gas mixture	Air	Air + N_2	Air + CO_2	Air
Concentration	20.95	18.93	1.13	0.034

Table III. Summary of steady-state chemostat measurements.

Chemostats	Dilution rate (h^{-1})	Biomass concentration (g/L)	OUR (mmol/gDW/h)	CER (mmol/gDW/h)
G1	0.051	14.03	1.61	1.60
G2	0.053	14.63	1.55	1.50
E1	0.053	14.69	1.51	1.49
E2	0.048	14.53	1.41	1.39

System Identification

A resting cell culture was obtained by switching off the medium feed to the chemostat. This resulted in both the OUR and CER to drop to very low levels (typically <5% of the chemostat reaction rates), and no significant change was observed during identification experiments.

A typical identification dataset is shown in Figure 4, from which the distortion of the off-gas measurements is clearly visible. A large number of models with different polynomial orders were evaluated. Model selection was carried out according to the following criteria:

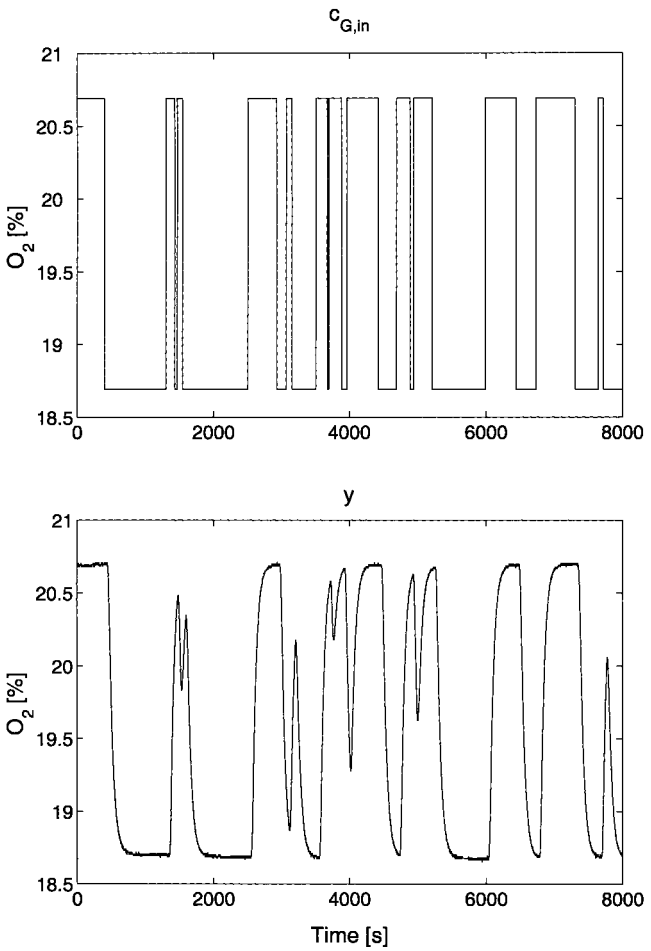

Figure 4. Input and output dataset for the identification of a transfer function.

- minimization of mean square prediction error (loss function);
- minimization of parameter confidence intervals;
- fit between the measured output and output simulated by the model;
- whiteness of the prediction errors (residuals);
- independence between the residuals and past inputs;
- a gain close to 1.

The parameters of the selected models and their confidence intervals are summarized in Table IV. The identified models give good descriptions of the off-gas system, as can be seen from the excellent agreement between the measurement and the simulation (Fig. 5).

Optimal Linear Filtering and Verification

The pulse responses in a time window of 150 s, as measured from the off-gas O_2 and CO_2 content and DO, are plotted in Figure 6 for glucose and ethanol pulses. It is obvious that the off-gas measurements are subject to a large time delay compared with the fast DO response. The (biomass specific) OUR and CER, estimated from off-gas measurements through the optimal filtering procedure, are plotted in Figures 7 and 8. Although the estimated OUR and CER from duplicate cultures are slightly different in magnitude, reproducibility of the trend is satisfactory, which is underlined by the reoccurring patterns.

The estimated OUR and CER can be verified by simulating the identified models with the estimated OUR and CER and compare the outputs, i.e., the simulated off-gas O_2 and CO_2 concentrations, with the measured ones. As can be seen from Figure 9, the simulated values fit closely to the measurements.

The initial response of the OUR following the glucose pulses shows a rapid increase followed by a sharp decrease within 50 s (see Fig. 7). This trend is not obvious in the off-gas O_2 measurement and contradicts what has been expected, i.e., a continuous increase until the capacity of the respiratory chain is saturated. However, the same trend can be observed in the available DO measurement, which supports the estimated initial sharp increase in OUR (as seen from a drop in DO), followed by a decrease in OUR (as seen from the increase in DO). To further confirm this, we simulated the DO corresponding to the estimated OUR during

Table IV. Polynomial coefficients and their standard deviations of identified transfer functions.

	O_2		CO_2	
a_1	−2.81	(±0.004)	−1.96	(±0.0002)
a_2	2.63	(±0.009)	0.96	(±0.0002)
a_3	−0.82	(±0.004)		
b_1	1.44×10^{-4}	($\pm 3.34 \times 10^{-6}$)	3.35×10^{-4}	($\pm 1.61 \times 10^{-6}$)
c_1	−0.56	(±0.01)	−0.23	(±0.008)
d_1	−0.98	(±0.003)	−0.98	(±0.002)
k	48		34	

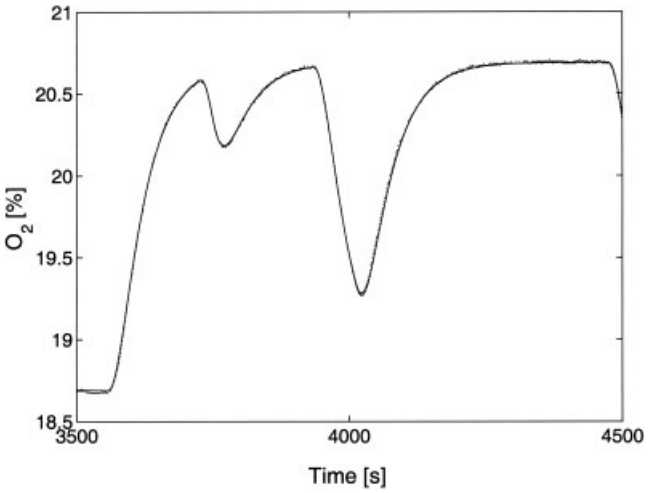

Figure 5. Model prediction (solid line) compared with measured output (dotted line) for an identified transfer function.

glucose and ethanol pulses, using the dynamic mass balances, Eqs. (1) and (2). In this calculation, the k_La is assumed to remain constant at the steady-state value k_La^0. As shown in Figure 10A, the pattern in the measured DO within 100 s after the pulse is structurally well matched by the simulated DO, which validates the unexpected trend in the

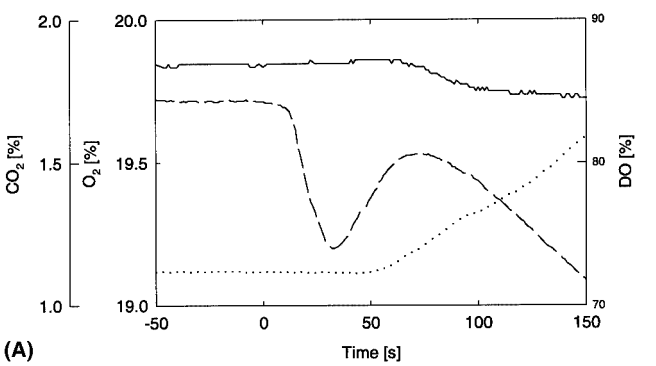

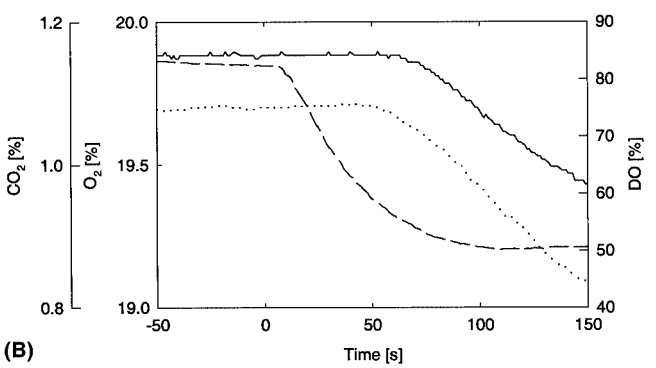

Figure 6. Off-gas and DO responses after a glucose pulse on chemostat G1 (**A**) and an ethanol pulse on chemostat E1 (**B**). The pulses were both given at $t = 0$. Solid line, O_2; dotted line, CO_2; dashed line, DO.

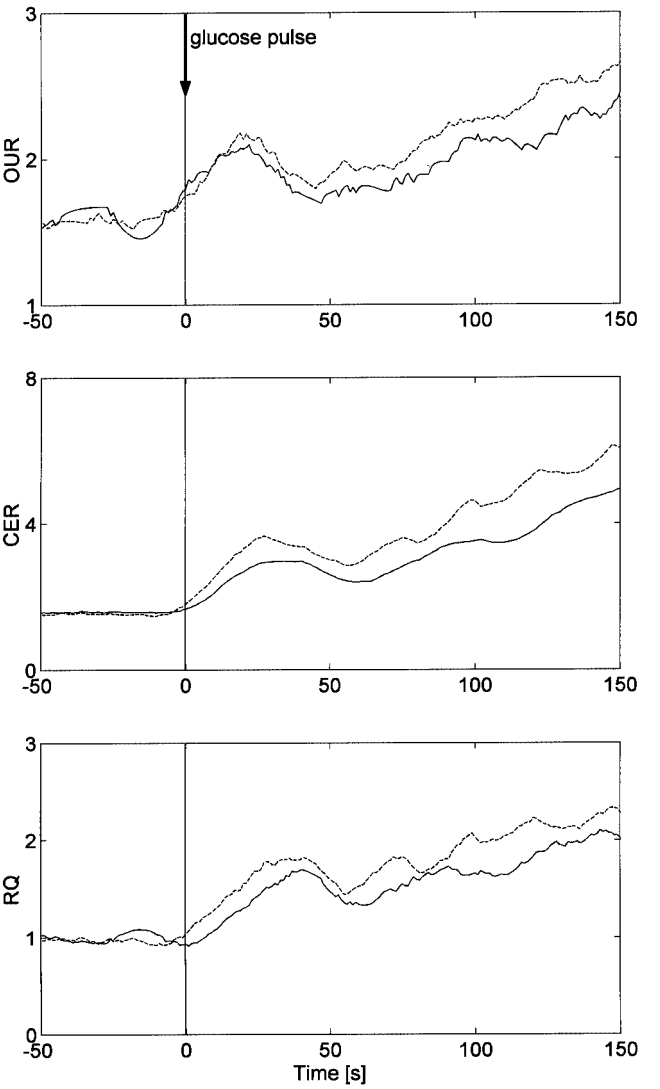

Figure 7. Estimated biomass specific OUR and CER in mmol/g DW/h during glucose pulses on chemostat G1 (solid line) and chemostat G2 (dashed line). The pulses were given at $t = 0$. For OUR, $\rho = 0.01$, $m - k = 20$; for CER, $\rho = 0.001$, $m - k = 20$.

estimated OUR in the glucose pulses. The same agreement between the measured and simulated DO is shown in Fig. 10B for an ethanol pulse. The pattern of estimated OUR is thus consistent with the independent DO measurement.

It should be emphasized that the DO measurement has neither been part of the identified model nor is it used for the OUR calculation. Further, the DO data is not corrected for possible dynamics of the DO probe. This partially explains the deviation of the simulated DO from the measured values in Figure 10. As for the glucose pulses, this deviation amplifies from 100 s onward. An explanation could be an increase of k_La after the glucose pulse, due to a release of surface-active compounds by the cells. Although we were unable to determine k_La during the highly dynamic period immediately after the pulse, the "apparent" k_La values is calculated from Eq. (1) by assuming a pseudo steady state after approximately 7 min after the pulse, the result of which suggests a non-constant k_La during glucose pulses (Fig. 11).

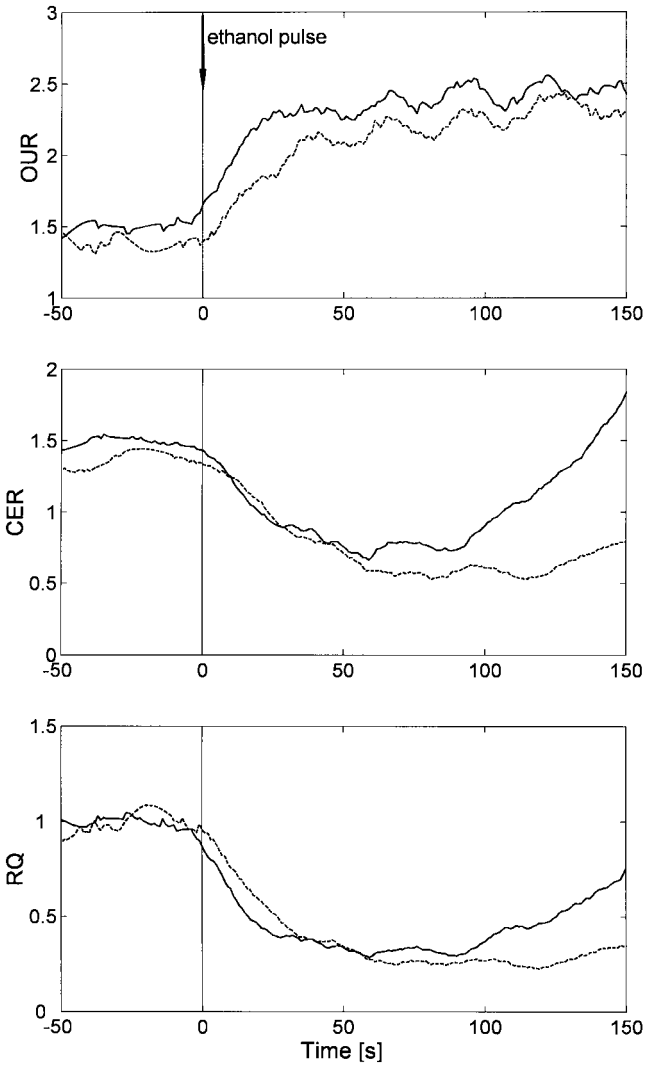

Figure 8. Estimated biomass specific OUR and CER in mmol/g DW/h during ethanol pulses on chemostat E1 (solid line) and chemostat E2 (dashed line). The pulses were given at $t = 0$. For OUR, $\rho = 0.01$, $m - k = 20$; for CER, $\rho = 0.001$, $m - k = 20$.

Because a constant k_La has been assumed in the modeling procedure and embedded in the identified transfer functions, it is important to access the error in the estimated OUR caused by possible changes in k_La during pulse experiments. The error ε can be expressed as

$$\varepsilon = r_{k_La} - r_{k_La^0} \tag{25}$$

r_{k_La} is the OUR calculated from a true, possibly varying k_La, while $r_{k_La^0}$ denotes the current OUR estimate with a constant k_La assumption. It is shown in Appendix 2 that ε is within 2% of the current OUR estimate.

The discrepancy between the estimated and simulated DO values and the relatively small error in the estimated OUR can be interpreted as follows: an increase in k_La would, in view of the low solubility of O_2, immediately lead to a large increase in the dissolved oxygen concentration, while the O_2 concentration in the gas phase, and hence in the off-gas, is only slightly affected. Thus, the constant k_La assumption would have resulted in an erroneous OUR estimation if based solely on DO measurement. In the case of CER, the influence of k_La is even less, due to the high

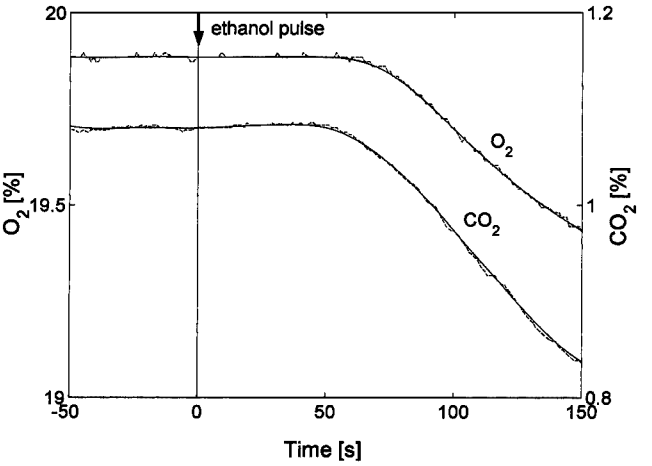

Figure 9. Simulated (solid line) and measured (dotted line) off-gas O_2 and CO_2 concentrations during an ethanol pulse on the chemostat E1. The pulse was given at $t = 0$.

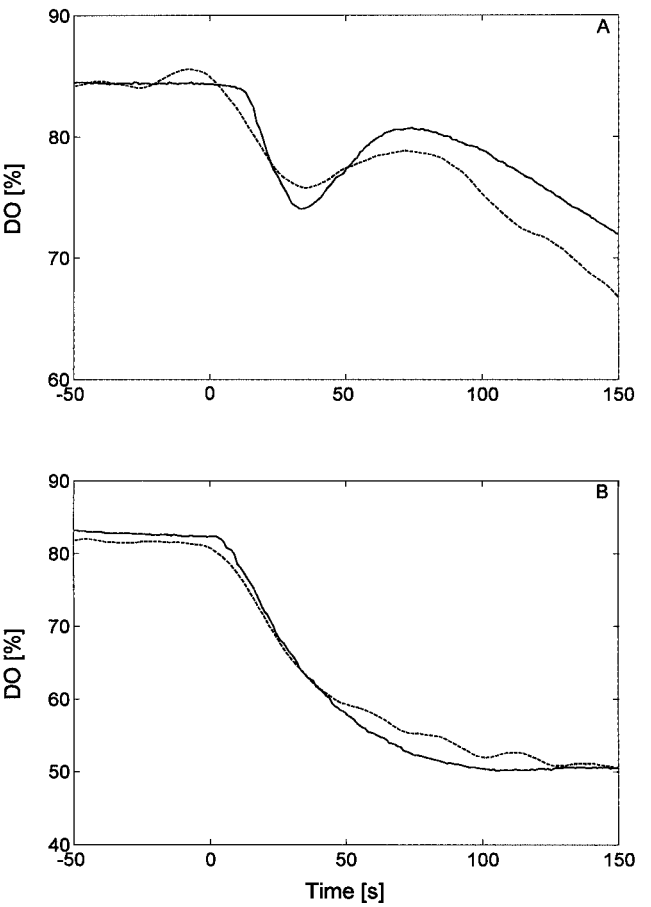

Figure 10. Simulated (dashed line) and measured (solid line) DO during a glucose pulse in chemostat culture G1 (**A**) and an ethanol pulse in chemostat culture E1 (**B**). The plotted measured DO is corrected for a delay of 5 s.

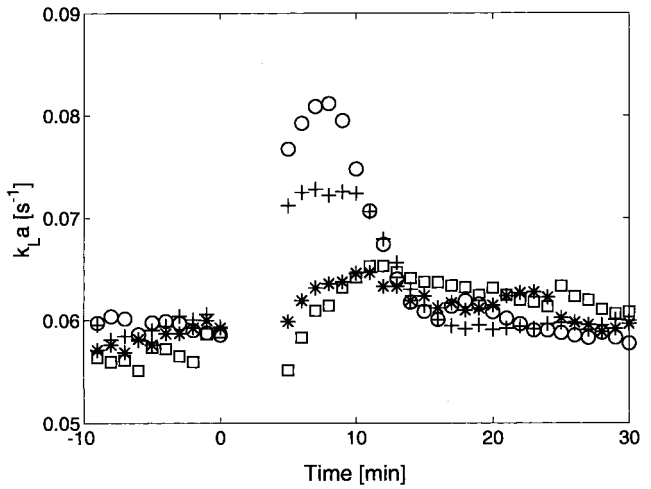

Figure 11. Apparent $k_L a$ based on pseudo steady-state assumption. The calculation is left out within 7 min after the addition of pulse substrate due to the dynamic nature: G1 (+), G2 (○), E1 (❄), E2 (□).

solubility of CO_2, which strongly reduces the changes in the driving force

$$\left(\frac{c_G}{m}\frac{P}{P_0} - c_L\right)$$

during a pulse. This can be an advantage of estimating OUR and CER using off-gas measurements only, in cases when $k_L a$ is likely to vary and cannot be accurately determined.

Transient OUR and CER Responses

Two distinct types of response in the direct measurements were triggered by glucose and ethanol as pulse substrate (Fig. 6). Both the off-gas O_2 concentration and DO drop shortly after the addition of either glucose or ethanol. This indicates a rapid initial oxygen uptake, which is confirmed by the OUR estimates. The off-gas CO_2 concentration, however, shows a different trend: it increases during the glucose pulse but decreases initially during the ethanol pulse.

The complexity of the in vivo dynamic behavior during a pulse is better demonstrated by the transient OUR and CER responses. For both glucose pulses (Fig. 7), the OUR showed a rapid increase of 50% within 25 s, probably due to the direct oxidation of cytosolic NADH produced in the glycolysis. The CER rose about 100%, leading to an RQ close to 2. This indicates ethanol formation, which is confirmed by the measured extracellular ethanol concentration (results not shown). After 25 s both OUR and CER decreased, followed by a gradual increase starting from 55 s. The reason of this unexpected decrease of both OUR and CER is yet unclear and is subject to further investigation.

For both ethanol pulses (Fig. 8), again an initial increase of the OUR was observed, which is of the same magnitude and speed as that observed for the glucose pulse experiments. Contrary to the glucose pulse experiments, the OUR remained at an elevated level thereafter and increased within 150 s toward a plateau of about 2.5 mmol/g DW/h, a value which was also reached in a glucose pulse. However, the CER showed a large unexpected decrease after the ethanol addition and started to increase only after 90 s. A possible explanation for the decrease of CER could be as follows: the cytosolic and mitochondrial pyridine nucleotide pool become fully reduced, due to the rapid oxidation of ethanol by alcohol dehydrogenase. This results in a very low level of NAD^+, which is a substrate of the TCA cycle. A temporary cessation of the TCA cycle would thus lead to the decrease in CER.

CONCLUSION

A new method has been developed to estimate the OUR and CER under highly dynamic conditions, taking into account the delay and distortion effects of the off-gas system. The mathematical formulation of the off-gas system, along with the black box simplification of Eq. (11), is verified by the capability of identified models to correctly describe the system response. The linear filtering procedure provides subsequently the OUR and CER estimates, which is consistent with the independent DO measurement and insensitive to $k_L a$ variations. Good reproducibility of estimated in vivo OUR and CER is observed between duplicate cultures.

Distinct types of responses were observed after the addition of either glucose or ethanol as pulse substrate to steady-state cultures of *S. cerevisiae* grown aerobically on glucose. The dynamics of OUR and CER during glucose and ethanol pulses are resolved for the first time within a time frame of 150 s and reveal a complex interplay between various parts of the primary metabolism, which cannot yet be adequately accounted for by our current knowledge of its kinetic behavior. The development of reliable in vivo kinetic models of microbial metabolism will be strongly benefited by the incorporation of this valuable information, in addition to the measured response of the intra- and extracellular metabolite concentrations.

NOMENCLATURE

A, B_1, B_c, B_r, C, D, F, G, G_c,G_d, G_r, H, M, N, Q, R	transfer functions in s or q	
a, b, c, d	polynomial coefficients	
B_2, B_r, G_n	scalars in transfer functions	
c	concentration of O_2 or CO_2	(mol/m^3)
e	zero-mean white noise	
$\mathcal{G}$	gain of transfer function	
k	time delay	(s)
$k_L a$	volumetric mass transfer coefficient	(s^{-1})
m	smoothing lag	(s)
m	equilibrium constant	
N	number of CSTRs in series	
n_a, n_b, n_c, n_d	order of transfer functions $A(q)$, $B(q)$, $C(q)$, and $D(q)$	
P	pressure in the fermentor	(bar)
P_0	ambient pressure	(bar)

p	nonswitching probability	
q	forward shift operator	
r	reaction rate (OUR or CER)	(mol/m^3/s)
T	sampling interval	(s)
T_b	length of basic switching interval	(s)
T_{sw}	expectation of the switching interval	(s)
u	input	
V	volume	(m^3)
v	zero-mean white noise	
x	measured off-gas concentration, undelayed	(mol/m^3)
y	measured off-gas concentration, delayed	(mol/m^3)
z	complex argument in z transform	
ε	estimation error	
ε_G	gas hold-up	
λ_e, λ_v	variance of white noise e and v	
ρ	signal to noise ratio	
τ_i, $i = 1, \ldots, N$	residence time in CSTRs in series	(s)
τ_a	first-order time constant of off-gas analyzer	(s)
τ_G	gas residence time	(s)
τ_s	99% settling time	(s)
Φ	flow rate	(m^3/s)

Subscripts

G	gas phase
L	liquid phase
in	gas or medium feed

Superscripts

$'$	change with respect to steady state
0	steady-state value
c	transfer function for input gas concentration
r	transfer function for reaction rate

APPENDIX 1

$$B_1(s) = \frac{1}{\varepsilon_G}\left[s + \frac{k_L a}{\tau_G}\right], \quad B_2 = \frac{1}{\varepsilon_G} k_L a,$$

$$F(s) = s^2 + \left[k_L a + \frac{1}{\varepsilon_G \tau_G} + \frac{k_L a P_0}{\varepsilon_G m P}\right] s + \frac{k_L a}{\varepsilon_G \tau_G}, \quad \text{and}$$

$$G_n = \frac{1}{\tau_a}\prod_{i=1}^{N}\frac{1}{\tau_i}, \quad G_d(s) = \left(s + \frac{1}{\tau_a}\right)\prod_{i=1}^{N}\left(s + \frac{1}{\tau_i}\right).$$

The hold-up ε_G is defined as V_G/V_L, and τ_G is defined as V_L/F_G.

APPENDIX 2

The estimation error made by constant $k_L a$ assumption is given by

$$\varepsilon = r_{k_L a} - r_{k_L a^0} \tag{2.1a}$$

Subtracting steady-state levels yields

$$\varepsilon = r'_{k_L a} - r'_{k_L a^0} \tag{2.1b}$$

where the prime denotes a deviation from the steady state.

A useful expression to access the magnitude of ε can be derived as follows. In the noise-free case ($\rho = 0$), the optimal filter reduces to a simple inversion of the transfer function G_r:

$$r'(s) = \frac{1}{G_r(s)}\, y'(s) \tag{2.2}$$

Eq. (2.2) can be divided into two separate steps: first, c'_G is derived from y' by inverting Eq. (6c). This step is not dependant on $k_L a$, since the transfer functions in Eq. (6c) do not contain any $k_L a$-dependent terms. The reaction rate r' can then be obtained from c'_G by combining mass balances, Eqs. (1) and (2):

$$r' = \frac{dc'_L}{dt} - \left[\Phi_G c'_G + V_G \frac{dc'_G}{dt}\right]\frac{1}{V_L} \tag{2.3}$$

Canceling terms containing c'_G in Eq. (2.3) yields

$$\varepsilon = r'_{k_L a} - r'_{k_L a^0} = \frac{dc'_{L,k_L a}}{dt} - \frac{dc'_{L,k_L a^0}}{dt} \tag{2.4}$$

Here $c'_{L,k_L a}$ is the actual liquid phase concentration, subject to a varying $k_L a$, while $c'_{L,k_L a}{}^0$ denotes the liquid phase concentration if $k_L a$ were constant.

When process and measurement noise is present, estimation of ε is made possible by taking the measured and simulated dissolved oxygen concentration in Figure 11 as approximations for $c_{L,k_L a}$ and $c_{L,k_L a}{}^0$, respectively. The latter approximation is allowed by realizing that the estimated reaction rate ($\hat{r}'$) corresponds exactly to $r'_{k_L a}{}^0$. Numerical differentiation of both quantities shows that the error never exceeds 2% of the estimated OUR within 150 s after the pulse.

REFERENCES

Ahlén A, Sternad M. 1989. Optimal deconvolution based on polynomial methods. IEEE trans on acoustic, speech and signal processing 37: 217–226.

Bailey JE. 1998. Mathematical modeling and analysis in biochemical engineering: past accomplishments and future opportunities. Biotechnol Prog 14:8–20.

Carlsson B, Lindberg C-F, Hasselblad S, Xu S. 1994. On-line estimation of the respiration rate and the oxygen transfer rate at Kungsängen wastewater treatment plant in Uppsala. Water Sci Technol 30:255–263.

Gombert AK, Nielsen J. 2000. Mathematical modelling of metabolism. Curr Opin Biotechnol 11:180–186.

Grewal MS, Andrews AP. 1993. Kalman filtering: theory and practice. Edgewater Cliffs, NJ: Prentice Hall.

Holmberg U, Olsson G. 1989. Simultaneous DO control and respiration estimation. Water Sci Technol 21:1185–1195.

Lessard P. 1996. Metabolic engineering: the concept coalesces. Nat Biotechnol 14:1654–1655.

Lindberg C-F, Carlsson B. 1996. Estimation of the respiration rate and oxygen transfer function utilizing a slow DO sensor. Water Sci Technol 33:325–333.

Ljung L. 1987. System identification: theory for the user. Edgewater Cliffs, NJ: Prentice Hall PTR.

Pattison RN, Swamy J, Mendenhall B, Hwang C, Frohlich BT. 2000. Measurement and control of dissolved carbon dioxide in mammalian cell culture processes using an in situ fiber optic chemical sensor. Biotechnol Prog 16:769–774.

Rizzi M, Baltes M, Theobald U, Reuss M. 1997. In vivo analysis of

metabolic dynamics in *Saccharomyces cerevisiae*. II. Mathematical model. Biotechnol Bioeng 55:592–608.

Royce PNC, Thornhill NF. 1991. Estimation of dissolved carbon dioxide concentrations in aerobic fermentations. AIChE J 37:1680–1686.

Spanjers H, Olsson G, Klapwijk A. 1994. Determining short-term biochemical oxygen demand and respiration rate in an aeration tank by using respirometry and estimation. Water Res 28:1571–1583.

Teusink B, Passarge J, Reijenga CA, Esgalhado E, van der Weijden CC, Schepper M, Walsh MC, Bakker BM, van Dam K, Westerhoff HV, Snoep JL. 2000. Can yeast glycolysis be understood in terms of in vitro kinetics of the constituent enzymes? Testing biochemistry. Eur J Biochem 267:5313–5329.

Theobald U, Mailinger W, Baltes M, Rizzi M, Reuss M. 1997. In vivo analysis of metabolic dynamics in *Saccharomyces cerevisiae*. I. Experimental observations. Biotechnol Bioeng 55:305–316.

Tulleken HJAF. 1990. Generalized binary noise test-signal concept for improved identification-experiment design. Automatica 26:37–49.

Vaseghi S, Baumeister A, Rizzi M, Reuss M. 1999. In vivo dynamics of the pentose phosphate pathway in *Saccharomyces cerevisiae*. Metab Eng 1:128–140.

Verduyn C, Postma E, Scheffers WA, Van Dijken JP. 1992. Effect of benzoic acid on metabolic fluxes in yeasts: a continuous-culture study on the regulation of respiration and alcoholic fermentation. Yeast 8: 501–517.

Visser D, van der Heijden R, Mauch K, Reuss M, Heijnen S. 2000. Tendency modeling: a new approach to obtain simplified kinetic models of metabolism applied to *Saccharomyces cerevisiae*. Metab Eng 2: 252–275.

Wright BE, Butler MH, Albe KR. 1992. Systems analysis of the tricarboxylic acid cycle in *Dictyostelium discoideum*. I. The basis for model construction. J Biol Chem 267:3101–3105.